An Alternate Technique for Near-Sun Ranging

J. W. Layland
Communications Systems Research Section

Measurement of the round-trip propagation time to a spacecraft when the signal path passes close by the sun is a severe challenge because of the high noise and time-varying signal delay encountered. Scintillation in the solar corona widens the spectrum of the received carrier signal so that it can not be efficiently tracked by the conventional phase locked receivers of the DSN. A substantial improvement in performance can be achieved by matching the processing bandwidth to the dynamical conditions of the near-Sun signal path. This processing can be performed off-line with software after the signal is open-loop digitized and recorded. This article gives a detailed description and estimates the performance of such a system.

I. Introduction

Measurement of round-trip propagation time to a spacecraft when the signal path passes close by the Sun is interesting for the physics that it measures and for the challenge it represents to communications. Zygielbaum (Ref. 1) has recently described the techniques that are currently being used successfully to make such measurements. In the light of his review, it is incumbent upon us to ask if there are any alternate techniques which can improve the quality of results. The answer appears to be a substantial yes when we match our processing bandwidths and probing waveforms precisely to the dynamical conditions of the near-Sun signal path.

II. The Receiver Structure

Figure 1 is a rough block diagram showing the geometry and the real-time portions of the near-Sun ranging system. The transmitter portion is identical to that of our current ranging systems with the possible exception of the range-code bandwidths, which will be discussed later. The receiver portion is based upon that of our current ranging systems, but some operations are deferred to nonreal-time by sampling and recording after the signal bandwidth is reduced to that of the spectral spreading caused by the near-Sun environment. Some items of equipment are needed which are not part of the current R&D ranging system (MU-II) or the Operational Ranging System. The more significant of these are indicated in Figure 1.

The receiver Local Oscillator (LO) is driven by a programmed oscillator, or (optionally) by a frequency tracking loop to place the middle of the received carrier spectrum essentially at the middle of IF passband. The LO frequency should be stable enough and precise enough that the bandwidth of the carrier signal at IF (as measured from the IF passband center) is indistinguishable from the bandwidth of the RF carrier as received. This cannot be accomplished by a conventional phase locked loop which must have a bandwidth comparable to the spectral spread in the received carrier.

Extraction of the carrier reference phase for coherent detection of the range-code sidebands can be performed in a near-optimal manner from the recorded quadrature samples of the carrier signal.

The receiver coder is not rate-aided by the estimate of its doppler frequency in real time, so that once synchronized with the transmitter, it remains so throughout the tracking operation. The range-code doppler should in all cases be much less than the spread-carrier bandwidth, so that correction for the range-code doppler can be applied without loss to the recorded quadrature samples of the detected range code.

We expect two principal benefits with the nonreal-time processing: (1) the carrier phase reference for the i^{th} sample can be extracted from an optimally weighted sum of the j^{th} carrier samples for all j in the range $i - k \leqslant j \leqslant i + k$, where the weighting values, and the memory-limit k depend upon the autocorrelation function (hence bandwidth) of the received carrier phase. Since this carrier reference is constructed using the j^{th} samples for $j > i$, as well as for $j < i$, there is potentially a 3-dB improvement in the SNR of this phase reference relative to an ideally matched phase-locked loop which must depend only upon signal received prior to the sample of interest, i.e., for $j < i$ only. In addition, the nonreal-time phase reference need not suffer the 1-dB limiter suppression factor present in the DSN tracking loops. While such small factors would not be important if the phase-reference had high SNR, they add directly to data SNR when the phase reference has below unity SNR.

(2) The phase of the range coders can be completely accounted for throughout the tracking pass. This means that if it is necessary, data from the entire pass can be accumulated to provide one range acquisition, rather than depending upon a complete short acquisition falling within favorable signal conditions. DRVID can be obtained by postprocessing whenever the signal is strong enough for the doppler data to be valid, and strong enough for the received range code phase to be tracked as a function of time.

Without the rate-aiding of the range coders from doppler data, the bandwidth of the range code used need only be set low enough to accommodate changes in group delay which result from charged particle density changes. Were rate-aiding by doppler to be used, the allowed range code bandwidth would be reduced by 1/2 to accommodate changes in the difference between group delay and phase delay.

III. Nonreal-Time Processing

The equations which follow describe the nonreal-time processing. Let the signal as received at the antenna be $r(t)$:

$$r(t) = n(t) + \alpha \sin \left\{ \omega_c [t - \eta(t)] + m \square \cos \left(\omega_m [t - \eta'(t)] + \phi_m \right) + \phi_c \right\} \quad (1)$$

In Equation (1), $n(t)$ is additive noise, α is signal amplitude, ω_c is carrier frequency, $\eta(t)$ is the time-varying phase delay, m is the range-code modulation index, ω_m is the range-code frequency, $\eta'(t)$ is the time varying group delay, and ϕ_m and ϕ_c are arbitrary phase-shifts on modulation and carrier. Let the code-reference waveforms be unit power sinusoids: $\sqrt{2}$ {sin/cos} $(\hat{\omega}_m t)$; and let the carrier-reference waveforms be unit power sinusoids: $\sqrt{2}$ {sin/cos}$(\hat{\omega}_c t)$. With no code rate-aiding, $\hat{\omega}_m$ will differ from ω_m primarily by the doppler on ω_m; $\hat{\omega}_c$ should differ from ω_c by the error in predicting (tracking) carrier doppler.

Only the difference-frequency terms of the cross products between $r(t)$ and the reference signals will be considered because sum-frequency terms are filtered out in processing. The low-frequency terms which appear integrated at points a and b of Figure 1 are

$$\frac{\alpha}{\sqrt{2}} \cos(m) \begin{Bmatrix} \sin \\ \cos \end{Bmatrix} ([\omega_c - \hat{\omega}_c]\, t - \omega_c \eta(t) + \phi_c) + \begin{Bmatrix} n_{1c}(t) \\ n_{1s}(t) \end{Bmatrix} \quad (2)$$

The low-frequency terms which appear integrated at points c through f of Figure 1 are

$$\frac{\alpha}{2} \sin(m)\, \xi \begin{Bmatrix} \cos \\ \sin \end{Bmatrix} ([\omega_m - \hat{\omega}_m]\, t - \omega_m \eta'(t) + \phi_m) \times \begin{Bmatrix} \cos \\ \sin \end{Bmatrix} ([\omega_c - \hat{\omega}_c]\, t - \omega_c \eta(t) + \phi_c) + \begin{Bmatrix} n_{cc}(t) \\ n_{cs}(t) \end{Bmatrix} \text{ or } \begin{Bmatrix} n_{sc}(t) \\ n_{ss}(t) \end{Bmatrix} \quad (3)$$

The factor ξ is the amplitude of the sine-wave fundamental of a squarewave. If $n(t)$ can be assumed to be white and Gaussian with spectral density N_0, the six noise terms in Equations (2) and (3) are also white, Gaussian, and independent, with density N_0. By earlier assumption, the bandwidths of the signal terms in Equations (2) and (3) are the same as the bandwidth

of the spread-carrier. These signals are integrated (or low-pass filtered) suitably for that bandwidth and then sampled and recorded for final processing later.

If the one-sided half-power bandwidth of the carrier spectrum is 120 Hz, we should be able to recover virtually all of the signal power by filtering each of the six signals to 250 Hz and sampling at 500 Hz. Since these signals are composed predominantly of Gaussian noise, quantization to 8 bits for each sample is more than adequate. This yields a recording rate of about 25 kb/s, so that a standard 730-m (2400-ft) reel of magnetic tape could record in excess of an hour of data. This record rate could probably be cut by a factor of four, through coarser quantization or narrow filtering, with only minor degradation.

For simplicity of exposition in what follows, the sampled signals will be assumed to be Nyquist-rate samples of both noise and signal processes. Modifications necessary to account for the actual spectrum of the carrier are straight-forward and not discussed. Let $\Psi_{ci} = [\omega_c - \hat{\omega}_c]\ t_i - \omega_c \eta\ (t_i) + \phi_c$ be the carrier phase at time t_i, $\Psi_{mi} = [\omega_m - \hat{\omega}_m]\ t_i - \omega_m \eta'(t_i) + \phi_m$ be the range-code phase at time t_i, and denote the various noises at time t_i by $n_{xi} = n_x(t_i)$ where x ranges over the various noise subscripts in Equations (2) and (3). The sequence $\{\Psi_{mi}\}$ contains the desired range information. The sequence $\{\Psi_{ci}\}$ contains little or no useful information because of the fluctuations in $\eta(t)$. The six samples at time t_i (subscript i assumed) are

$$\begin{aligned}
\beta_{1c} &= \frac{\alpha}{\sqrt{2}} \cos(m) \sin(\Psi_c) + n_{1c} \\
\beta_{1s} &= \frac{\alpha}{\sqrt{2}} \cos(m) \cos(\Psi_c) + n_{1s} \\
\beta_{cc} &= \frac{\alpha}{2} \sin(m)\, \xi \cos(\Psi_m) \cos(\Psi_c) + n_{cc} \\
\beta_{cs} &= \frac{\alpha}{2} \sin(m)\, \xi \cos(\Psi_m) \sin(\Psi_c) + n_{cs} \\
\beta_{sc} &= \frac{\alpha}{2} \sin(m)\, \xi \sin(\Psi_m) \cos(\Psi_c) + n_{sc} \\
\beta_{ss} &= \frac{\alpha}{2} \sin(m)\, \xi \sin(\Psi_m) \sin(\Psi_c) + n_{ss}
\end{aligned} \tag{4}$$

Information about the sequence $\{\Psi_{ci}\}$ can be conveniently destroyed by taking cross products of the βs.

$$\begin{aligned}
\beta'_c &= \beta_{cc} \cdot \beta_{1s} + \beta_{cs} \cdot \beta_{1c} \\
\beta'_s &= \beta_{sc} \cdot \beta_{1s} + \beta_{ss} \cdot \beta_{1c}
\end{aligned} \tag{5}$$

Taking expected values,

$$\begin{aligned}
\langle \beta'_c \rangle &= \frac{\alpha^2}{2\sqrt{2}}\, \xi \sin(m) \cos(m) \cos(\Psi_m) \\
\langle \beta'_s \rangle &= \frac{\alpha^2}{2\sqrt{2}}\, \xi \sin(m) \cos(m) \sin(\Psi_m)
\end{aligned} \tag{6}$$

and if V denotes $\langle n_x^2 \rangle$ for any of the noise terms,

$$\begin{aligned}
\text{Variance}\ \{\beta'_c\} &= 2 \cdot V^2 + V \cdot \frac{\alpha^2}{4} \xi^2 \sin^2(m) \cos^2(\Psi_m) \\
&\quad + V \cdot \frac{\alpha^2}{2} \cos^2(m) \\
\text{Variance}\ \{\beta'_s\} &= 2 \cdot V^2 + V \cdot \frac{\alpha^2}{4} \xi^2 \sin^2(m) \sin^2(\Psi_m) \\
&\quad + V \cdot \frac{\alpha^2}{2} \cos^2(m)
\end{aligned} \tag{7}$$

The β'_c, β'_s cross products are accumulated for as long as the variations in Ψ_m will permit in order to estimate the range information which is in Ψ_m. The amplitude SNR of β'_c is

$$\rho'_c = \frac{\frac{\alpha \cos(m)}{\sqrt{2V}} \cdot \frac{\alpha \sin(m)}{\sqrt{4V}}\, \xi \cos(\Psi_m)}{\sqrt{2 + \frac{(\alpha \cos(m))^2}{2V} + \frac{(\alpha \sin(m)\, \xi)^2}{4V} \cos^2(\Psi_m)}} \tag{8}$$

while that for ρ'_s is similar. If the carrier signal is strong relative to the noise, and the modulation index m is small, then ρ'_c converges to

$$\rho_c' \approx \frac{\alpha}{2\sqrt{V}} \sin(m) \cdot \xi \cdot \cos(\Psi_m) \quad \text{if } \alpha \cos(m) \gg \sqrt{V} \tag{9}$$

This result is identical to the comparable result for coherent detection when a strong carrier is tracked by a phase locked loop. If the total signal is weak relative to the noise, then ρ_c' is approximately

$$\rho_c' \approx \left(\frac{\alpha}{2\sqrt{V}}\right)^2 \cdot \cos(m) \cdot \sin(m) \cdot \xi \cdot \cos(\Psi_m) \quad \text{if } \alpha \ll \sqrt{V} \tag{10}$$

When a conventional phase locked loop tracks $\Psi_c(t)$, the loop SNR, R_L should be given by

$$R_L = \eta \frac{\alpha^2 \cos^2(m)}{2V} \tag{11}$$

Where η is a correction factor for the relative bandwidths of the tracking loop and the samples to be recorded (cf. Eq. (4)). By the bandwidth assumptions, $\eta < 1$. The information on cos (Ψ_m) is now contained in β_{cc}, which has expected value

$$\langle \beta_{cc} \rangle \approx \frac{\alpha}{2} \sin(m)\, \xi \cos(\Psi_m) \left[I_1(R_L)/I_0(R_L) \right] \tag{12}$$

The modified Bessel functions $I_i(\cdot)$ derive from the tracking error of a first-order phase locked loop following $\Psi_c(t)$. The weak-signal asymptote for the amplitude SNR of β_{cc} is:

$$\rho_{cc} \approx \left(\frac{\alpha}{2\sqrt{V}}\right)^3 \cdot \eta \cdot \sin(m) \cdot \xi \cdot \cos^2(m) \cdot \cos(\Psi_m) \quad \text{if } \alpha \ll \sqrt{V} \tag{13}$$

which may be very much less than ρ_c' for small α. The nonreal-time processing should thus perform much better than real-time coherent detection when the signal is weak, and at least as well when the carrier signal is strong.

IV. Ranging Link Design

Using the receiver structure described above, ranging link design is completed by specifying the bandwidth within which the signal must be measured to ensure reliable operation, and from this and the spectral broadening information, the bandwidth of the range code itself. Data from previous solar conjunctions will be used as a guide.

The three primary degradation terms are shown approximated in Figure 2 as a function of $\rho = R/R_\odot$, the distance from the Sun of the signal ray path at its closest approach, given in units of the solar radius. The approximations shown are slight over-estimates to actual data for $\rho > 1.7$. They are of dubious value for $\rho < 1.7$ where no data was found.

The receiver system temperature increases drastically as the antenna beam approaches the Sun's disk. Rockwell (Ref. 2) developed an approximation to the system temperature increase caused by close approach to the Sun which is

$$T_{\text{SUN}} \approx 5.6 \exp\{16.3/(\rho + 1)\}$$

when written in terms of ρ. His approximation is conveniently overestimated by

$$T'_{\text{SUN}} \approx 20 \cdot \left(\frac{\rho}{10}\right)^{-1.5} + 3 \cdot \left(\frac{\rho}{10}\right)^{-4} \tag{14}$$

This form is convenient for graphic display and "calculation" since it is representable as the sum of straight line segments on a log-log plot. In Figure 2, the asymptotes are shown for T_{SUN} in dB degradation relative to a nominal system temperature of 20 K.

Spectral spreading data has been presented by Woo (Ref. 3). This data is for one-way transmission at S-band with a variety of spacecraft, and a variety of ρ. The carrier spectrum is spread by scintillation into an almost Gaussian shape. The half-power bandwidth of this spread carrier is slightly overestimated by the function

$$B \approx 2 \left(\frac{\rho}{10}\right)^{-1.5} + 0.25 \left(\frac{\rho}{10}\right)^{-3.5} \tag{15}$$

This form is again chosen for graphic convenience. In Figure 2, B is shown in dB relative to 1 Hz.

Angular broadening of the ray-path from the Helios I spacecraft was inferred by Woo (Ref. 3) at $\rho = 1.7$. Assume that this

measurement is consistent with prior determinations at much larger ρ, at a similar "quiet" Sun condition. Then the factor by which the beam cross-section of the DSN 64-m antenna is exceeded is approximately

$$\text{Beam Overspread} \approx 10^3 \times \rho^{-9} + 1 \qquad (16)$$

when a 'moderate' solar activity is assumed. The S-band signal power loss due to this beam spreading is shown in dB in Figure 2.

Amplitude scintillations can also cause severe short-term degradation. However, most available literature seems to imply that the overall long-term effect can be almost negligible, so it is tentatively ignored here.

For the ranging link calculations, the bandwidths of the spread spectrum of the range code is proportional to that of the carrier on which it resides, but reduced by the ratio of the range code frequency to the carrier frequency. For two-way S-band transmission, the spectral spreading should be $\sqrt{2}$ times that for one-way S-band transmission.

For two-way S-band up/X-band down transmission, the spectral broadening takes place almost entirely on the S-band uplink. The received X-band carrier bandwidth will be 11/3 times that of the one-way S-band link as a result of the multiplication to the S-band frequency in the transponder. The range-code bandwidth will be essentially the same as for the one-way S-band link. The angular beam-spreading loss, which pertains to the down-link only, is reduced for X-band to $(3/11)^2$ times its S-band value.

An example link calculation has been carried out using power assumptions pertinent to the recent past Viking solar superior conjunction. Then, the undegraded down-link carrier power was approximately -143 dBm, and the ranging sideband power was approximately -153 dBm. These ranging sidebands consist mostly of a turned-around copy of the uplink range code whenever the S-band uplink is suitably strong relative to thermal noise at the spacecraft. Using these parameters, and a "strong uplink" assumption, the ranging link SNR is as shown in Figure 3 as a function of ρ for a two-way S-band link. Only the straight line asymptotes are shown. The ranging sideband power-to-noise density ratio (P_r/N_0) is shown in dB-Hz. When the solar impact parameter ρ is moderately large ($\rho > 10$), this ratio is approximately the same as it is far from the Sun. As ρ decreases below 10, the increased system temperature and beam-spreading losses cause severe degradation. The carrier sample SNR $(P_c/N_0 \cdot W_c^s)$ is shown in dB. The sample bandwidth is the two-way counterpart of the half-power bandwidth displayed in Figure 2, so that there is a 3-dB direct signal power loss incurred. As ρ decreases, the increase in sample bandwidth joins with increased system temperature and beam spreading losses to degrade the SNR as shown. The detected P_r/N_0 is that to be obtained through the quasi-coherent scheme described above, as represented by Eq. (8).

A ranging measurement SNR of +20 dB can be achieved at $\rho \approx 1.85$ by filtering this measurement to 10^{-2} Hz if significant power is not to be lost. From Figure 2, the half-power bandwidth of the S-band (2.3×10^9 Hz) carrier at $\rho = 1.85$ is 19.5 dB-Hz one-way (21 dB-Hz two-way). This spectral spread on a range code of 10^5 Hz or less will fit within a 10^{-2} Hz measurement bandwidth. For an S-band uplink/X-band downlink, the ranging link is as shown in Figure 4, as a function of ρ. This link appears to be operable at a somewhat smaller value of ρ than the two-way S-band link because the carrier bandwidth expansion due to frequency multiplication to X-band is more than counterbalanced by the lessened degradation of the X-band downlink.

The value of ρ for which ranging appears to become unworkable is in the vicinity of 1.8 to 1.9 with the assumptions used. The actual value will vary from this depending upon the activity level of the Sun, and the validity of the various assumptions and approximations. In particular, the assumed "strong" uplink is probably also degrading as ρ decreases, and this degradation would be reflected in a reduced P_r/N_0 in the downlink. This effect needs to be examined, but should not dramatically change the threshold value for ρ.

For conventional phase locked loop carrier tracking and coherent detection, and the assumptions of Figure 3 and Figure 4, the value of ρ for which ranging appears to become unworkable is in the vicinity of 2.0 for both S/S and S/X ranging links. In fact, the closest range point achieved to date was at $\rho = 2.0$ ($< \text{SEP} = 0.55°$) using the conventional DSN receiving equipment in conjunction with the Mu-II ranging system (Ref. 1).

V. Signaling Strategy

In practice, only a part of the ranging signal energy can be placed into the highest frequency code to be used. The remainder must be transmitted as lower frequency tones in order to resolve ambiguities in the measured range to at least the a priori uncertainty in that measurement. Suppose that overall one half of the signal energy is to be allocated to the highest frequency code for which spectral spreading is within the measurement bandwidth, and the other half allocated to

resolving ambiguities. This can be achieved conveniently in a sequential component system by dividing time into equal-length segments, e.g. 30 sec, and using every other segment for the high frequency code component. A signal received in several segments can be combined together as allowed by spectral spreading of that code component, and as needed from SNR considerations.

The remaining segments should be allocated to lower frequency range code components such that the entire measurement strategy is robust in the face of larger-than-expected variations in the plasma delay, and such that the a priori ambiguities can be resolved reliably. Let C_1 denote the highest frequency code component, and let C_1 be assigned to all even-numbered time segments. Two feasible signalling strategies for the odd-numbered segments are as shown in Table I, under the assumption that ambiguity can be resolved with only five code components. Note that at no time is a code "chopped" by a higher frequency code. The linear strategy is analogous to an acquisition as performed by current ranging systems, while the logarithmic strategy should be somewhat more tolerant of unexpected delay variations.

VI. Discussion

From the information in the preceding sections, it is clear that we can improve the performance of near-Sun ranging operations by quasi-optimal detection techniques that are possible with nonreal-time processing. This improvement would at least manifest itself by an increase in the reliability with which range data is obtained when the spacecraft signal passes to within a few solar radii of the Sun. Optimistically, we may be able to reduce the value of R at which ranging is accomplished to about 1.8 solar radii.

As dual-frequency range is a measure of the total charged particle content in the signal path, and the concurrent doppler or spectral spreading data provide a measure of the variations in that charged particle content, we will be testing very close to the Sun the often used assumption that the total charged particle content of the solar corona is directly proportional to its variation. Furthermore, since the data acquisition process "just runs" without the hectic scheduling activity normally associated with near-Sun ranging, the amount of operational trauma associated with solar-superior conjunction experiments should be greatly reduced.

References

1. Zygielbaum, A. I., "Near-Sun Ranging" DSN-PR 42-41, pp. 43-50, October 15, 1977. Jet Propulsion Laboratory, Pasadena, Calif.
2. Rockwell, S. T., "A model of SNR Degradation during Solar Conjunction", DSN-PR 42-38, pp. 187-198. April 15, 1977. Jet Propulsion Laboratory, Pasadena, Calif.
3. Woo, R. "Radial Dependence of Solar Wind Properties Deduced from Helios 1/2 and Pioneer 10/11 Radio Scattering Observations" (Preprint) 1977. *Astro Physics Journal*, January 1978.

Table 1. Signalling strategies

Time segment No.	1	3	5	7	9	11	13	15
Linear strategy	C_2	C_3	C_4	C_5	··· REPEAT ···			
Logarithmic strategy	C_2	C_3	C_2	C_4	C_2	C_3	C_2	C_5 ···

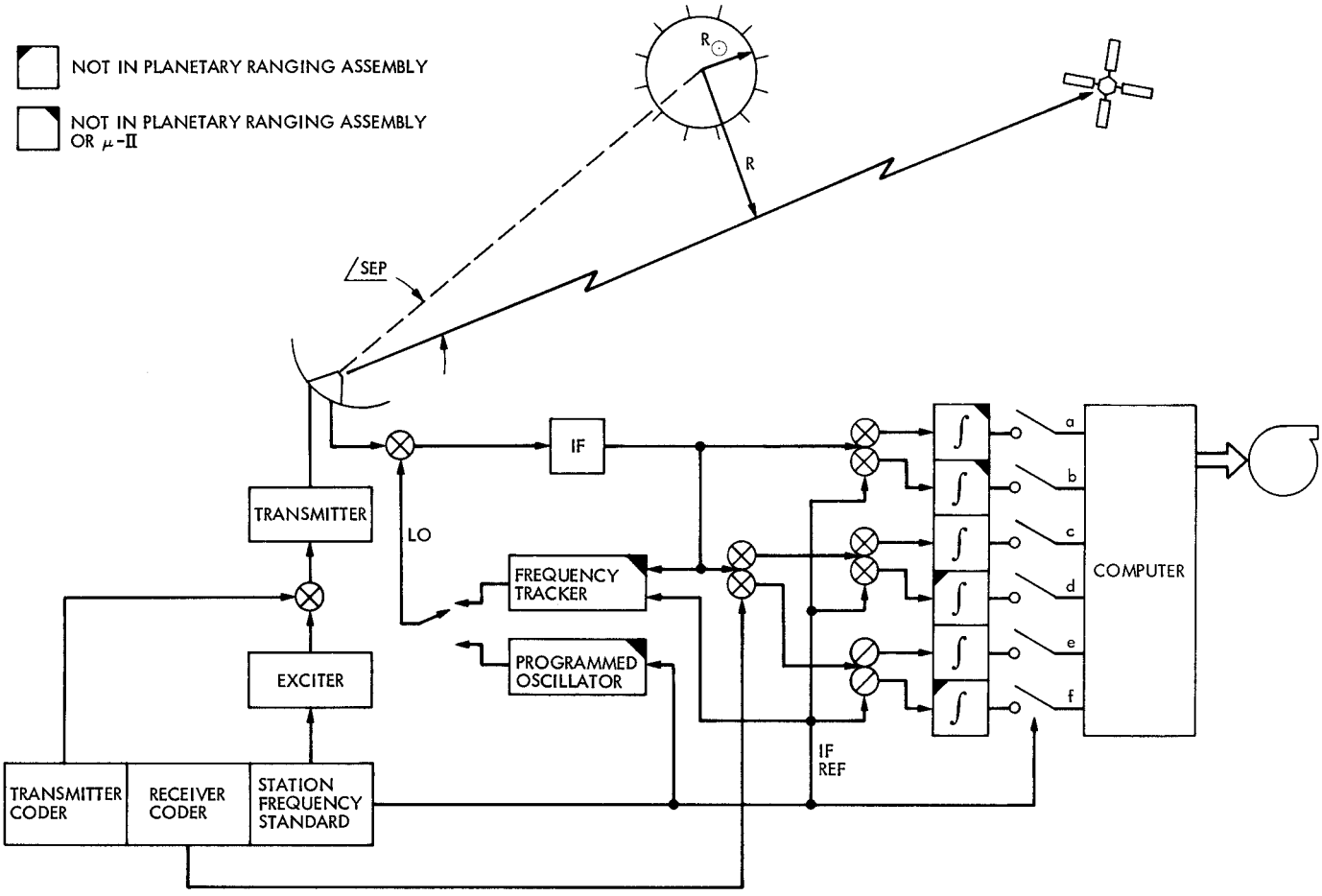

Fig. 1. Block diagram of near-Sun ranging system

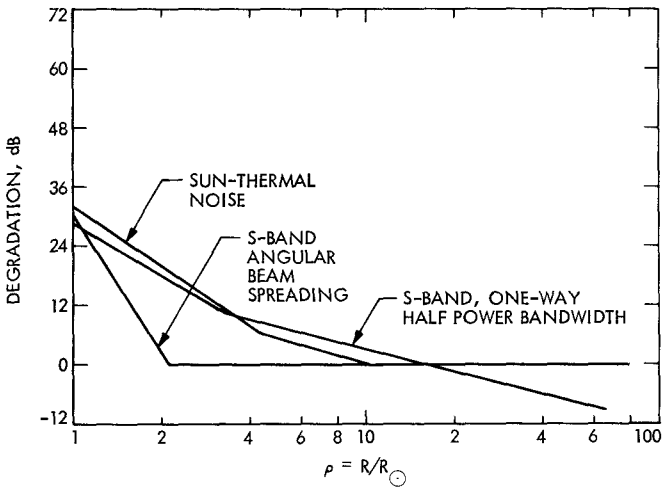

Fig. 2. Degradation terms for near-Sun ranging

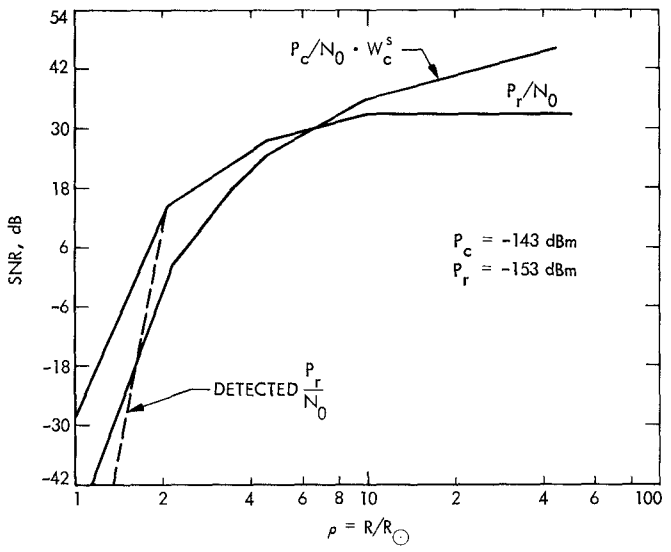

Fig. 3. Ranging link parameters two-way S/S

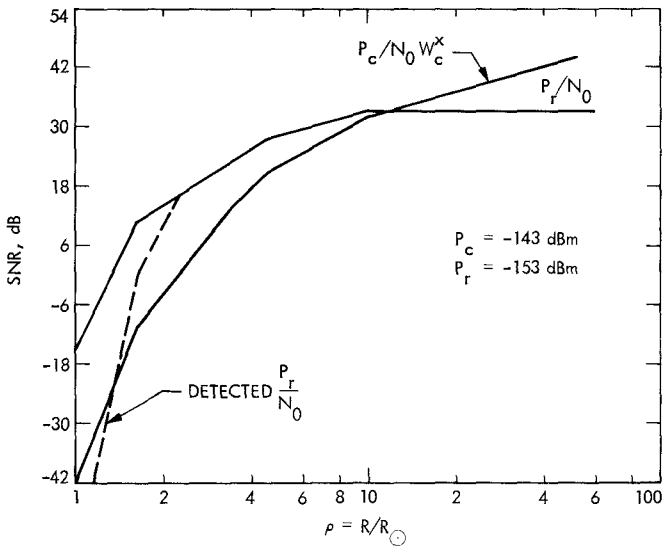

Fig. 4. Ranging link parameters two-way S/X